Reflective limiters based on self-induced violation of $\mathcal{CT}$ symmetry

Eleana Makri, Roney Thomas, and Tsampikos Kottos
Department of Physics, Wesleyan University, Middletown, Connecticut 06459, USA

(Received 6 October 2017; published 30 April 2018)

Non-Hermitian bipartite photonic lattices with charge-conjugation ($\mathcal{CT}$) symmetry can support resonant defect modes which are resilient to bipartite losses and structural imperfections. When, however, a (self-)induced violation of the $\mathcal{CT}$ symmetry occurs via tiny permittivity variations, the resonant mode is exposed to the bipartite losses and it is destroyed. Consequently, the transmission peak is suppressed while the reflectance becomes (almost) unity. We propose the use of such photonic systems as power switches, limiters, and sensors.

DOI: 10.1103/PhysRevA.97.043864

I. INTRODUCTION

Symmetries and their violations constitute an important theme of investigation, both for their own fundamental interest [1] and for their potential technological use in managing wave transport [2,3]. For example, the violation of time-reversal ($\mathcal{T}$) symmetry is a necessary condition for the realization of isolators and circulators [4–6]. Similarly, chiral ($\mathcal{C}$) [7–9] and charge-conjugation ($\mathcal{CT}$) symmetries [7] have been proven important for the realization of defect modes which are topologically protected against disorder and which potentially enable robust unidirectional transport, mode selectivity, etc. [10–22]. Originally these topologically protected defect states attracted attention due to their possible realizations in condensed matter systems [23–25]. Recently, classical wave physics setups—like photonics, acoustics, and microwaves—have been proven fertile platforms for the implementation of topological defect modes [18,26–29]. In all of these cases the topological protection invokes a combination of judicious band-structure designs and symmetry implementations [10–21]. Among the well-studied setups are coupled resonator optical (or microwave or acoustic) waveguide (CROW) arrays [18,20–22,26,29]. Extensions to non-Hermitian CROWs have also been considered and were shown to support nontrivial topologically protected defect modes [30–32]. Nevertheless, very few studies address the transport properties of these defect states once the system is coupled to leads [20,21,33,34].

Here, we design a family of $\mathcal{CT}$-symmetric non-Hermitian bipartite CROW arrays with (self-)regulated transport characteristics. These arrays consist of resonators with the same resonant frequencies but different linewidths. In the presence of a topological defect [18], the associated $\mathcal{CT}$-symmetric defect mode is strongly localized around the defect resonator and has nodal points at alternating resonators. This symmetry-induced staggered profile shields the defect mode from structural imperfections and from losses associated with the "nodal-point" resonators. We show that the symmetry protection pertains also to the case of scattering setups where the associated resonant defect mode has a similar staggered form—thus minimizing the interaction with the lossy "nodal-point" resonators and enforcing a high resonant transmission peak. We refer to this phenomenon as *symmetry-enforced transmittivity*. When, however, the defect resonator is made of a material with a permittivity that is sensitive to either self-induced heating due to high fluence of the incoming electromagnetic radiation, or to high intensity field values, the resonant defect mode experiences a $\mathcal{CT}$-symmetry violation. This self-induced explicit symmetry violation exposes the defect mode to the lossy "nodal-point" resonators, leading to its destruction together with the dramatic suppression of the associated resonant transmission. As a result, the entire structure becomes highly reflective at the resonant frequency. We propose to utilize the fragile nature of the resonant transport to $\mathcal{CT}$-symmetry violations in order to realize a different family of photonic limiters and switches [35,36].

The structure of the paper is as follows. In Sec. II, we present the proposed CROW microwave photonic limiter and its symmetries. We also discuss the consequences of these symmetries in the structure of the defect mode and its resulting robustness against structural imperfections. In Sec. III, we analyze the scattering setup and demonstrate the hypersensitive nature of the defect resonant transmission against self-induced (explicit) symmetry violations. In Sec. IV we analyze an on-chip version of the photonic limiter and demonstrate its efficiency against previous proposals. Finally, in Sec. V we present our conclusions.

II. DESIGN AND MODELING OF $\mathcal{CT}$-SYMMETRIC MICROWAVE CROWs

A design of our setup is shown in Fig. 1. It consists of a one-dimensional array of N resonators, which are arranged with alternating short (d_1) and long (d_2) distances from one another. We assume, without any loss of generality, that $N = 21$. A central dimerization defect at $n_0 = 11$, assumed to consist of a thermally (or intensity) modulated material, is introduced by repeating the spacing d_2 from the adjacent resonators on the left and right, respectively. The permittivity variation in the material making up the defect resonator ($n_0 = 11$) is assumed to be self-induced (e.g., via heating by the incident radiation or via the local field intensity). Representatives of such materials include germanium-antimony-tellurium alloys [37], oxides of vanadium, etc. [38,39]. The resonant frequency β_{n_0} of the defect resonator matches the frequencies of the other resonators, $\beta_n = \beta_0$. The two resonators on the left ($n = 10$)

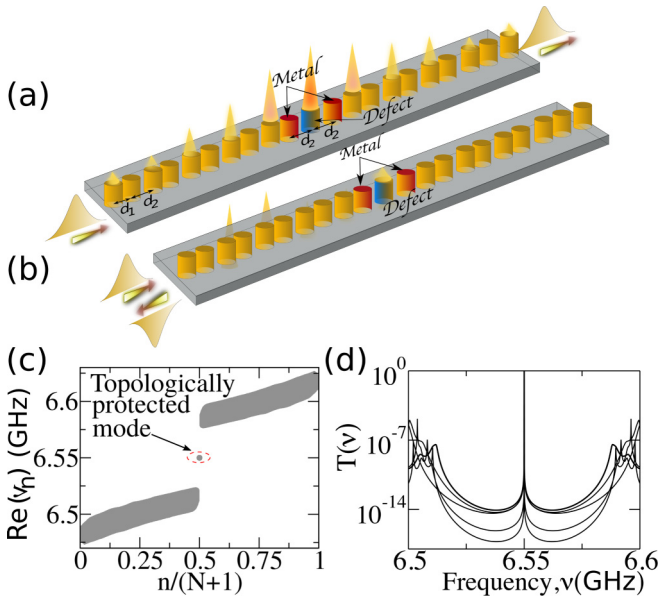

FIG. 1. (a) A $\mathcal{CT}$-symmetric microwave CROW array consisting of identical resonators separated with alternating distances $\boldsymbol{d_1}$ and $\boldsymbol{d_2}$. A central defect (blue), which contains a permittivity modulated material, is introduced by repeating $\boldsymbol{d_2}$. The two nearby resonators (red) have enhanced Ohmic losses (a). For weak signals the incident radiation is transmitted via a midgap resonant defect mode with a staggered profile (b). When $\mathcal{CT}$ violation is (self-)induced via permittivity variations of the central resonator, the structure operates as a broadband reflector. (c) The eigenfrequencies vs their respective indices for various disorder realizations of $\boldsymbol{d_1}$ and $\boldsymbol{d_2}$. The defect eigenmode (middle of the gap) is spectrally protected against disorder. The other modes are sensitive to $\boldsymbol{d_1}$ and $\boldsymbol{d_2}$ variations (shadowed area). (d) Transmittance for different positional realizations. The resonant peak is insensitive and spectrally protected.

and right ($n = 12$) of the central defect (see Fig. 1), involve large Ohmic losses. The losses are optimally managed in a way that these resonators maintain the same resonant mode as the other cavities—a condition that is necessary for $\mathcal{CT}$ symmetry—and at the same time overcome restrictions from the Kramers-Kronig relations. This can be achieved through deposition of thin layers of a metal on top of the resonators or by using an absorbing paint like graphite powder. The losses due to the coating will be reflected in the resonant frequencies of these resonators which acquire an imaginary part, i.e., $\beta_{10} = \beta_{12} = \beta_0 + i\gamma$. In our numerics, we have assumed that $\beta_0 = 6.55\,\text{GHz}$, $\gamma = 50\,\text{MHz}$, $t_1 = 50\,\text{MHz}$, and $t_2 = 10\,\text{MHz}$.

The array of Fig. 1 is described, in the resonant mode representation of the isolated resonators, by the following tight-binding Hamiltonian:

$$\boldsymbol{H} = \sum_{\boldsymbol{n}} \boldsymbol{\beta_n} |\boldsymbol{n}\rangle\langle\boldsymbol{n}| + \sum_{\boldsymbol{n}} \boldsymbol{t_n}(|\boldsymbol{n}\rangle\langle\boldsymbol{n}+\boldsymbol{1}| + |\boldsymbol{n}+\boldsymbol{1}\rangle\langle\boldsymbol{n}|), \quad (1)$$

where $n = 1, \ldots, N$ denotes the resonator index and $t_n = t_1$ or t_2 indicates the evanescent coupling strengths between the two nearby resonators [with their corresponding short (d_1) and long (d_2) distances, respectively]. When $\gamma = 0$, the Hamiltonian (1) is chiral symmetric, i.e., $\{\mathcal{C}, H\} = 0$ [40], where $\{\cdots\}$ indicates an anticommutation, and $C = P_{\text{even}} - P_{\text{odd}}$ is the chiral operator with $P_{\text{even/odd}} = \sum_{n\in\text{even/odd}} P_n$ and $P_n \equiv |n\rangle\langle n|$ is the projection to a specific site n. The eigenfrequencies ν_n of Hamiltonian (1) are real and occupy two bands, $\beta_0 - t_1 - t_2 < \nu < \beta_0 - |t_1 - t_2|$ and $\beta_0 + |t_1 - t_2| < \nu < \beta_0 + t_1 + t_2$, separated by a gap of width $\Delta \equiv 2|t_1 - t_2|$. The central unpaired eigenfrequency $\nu^D = \beta_0$ corresponds to a $\mathcal{C}$-symmetric defect eigenmode ψ^D which is localized at $n_0 = 11$. At the infinite-chain limit, the field amplitude ψ_n^D at the nth resonator takes the form

$$\boldsymbol{\psi}_{\boldsymbol{n}}^{\boldsymbol{D}} \sim \begin{cases} \frac{\mathbf{1}}{\sqrt{\xi}} \boldsymbol{e}^{-\frac{|\boldsymbol{n}-\boldsymbol{n_0}|}{\xi}}, & \boldsymbol{n} \text{ odd} \\ \mathbf{0}, & \boldsymbol{n} \text{ even} \end{cases}, \quad (2)$$

where $\xi = 1/\ln(t_1/t_2)$. Importantly, Eq. (2) indicates that this state is supported only by the odd n sublattice. Therefore, it is also an eigenstate of any diagonal operator $D_{\{n\in\text{even}\}} = \sum_{n\in\text{even}} c_n P_n$ (where c_n is a complex number), with associated zero eigenvalue.

When $\gamma \neq 0$, the Hamiltonian (1) becomes non-Hermitian and $\{\mathcal{C}, H\} \neq 0$; thus the system is no longer chiral symmetric. We find that H anticommutes with the charge-conjugation operator $\mathcal{CT}$, i.e., $\{\mathcal{CT}, H\} = 0$, where $\mathcal{C}$ is the unitary chiral symmetry operator (as defined above) and $\mathcal{T}$ is the time-reversal operator associated with complex conjugation operations. $\mathcal{CT}$ symmetry, also known as particle-hole symmetry, has recently been explored in the context of photonic systems [31,41] and has profound consequences on the spectrum of Eq. (1). The latter now consists of pairs of *complex* eigenfrequencies $\beta_0 + \delta\nu_n$, $\beta_0 - \delta\nu_n^*$, where $\delta\nu_n$ is a complex number. The (unpaired) defect mode ψ^D [see Eq. (2)] is an eigenstate of $D_{\{n=10,12\}} = i\gamma(P_{10} + P_{12})$, with corresponding zero eigenvalue, and thus it is also an eigenstate of the non-Hermitian Hamiltonian (1) $H(\gamma) = H(0) + D_{\{n=10,12\}}$ with an eigenfrequency $\nu^D = \beta_0$.

In order to verify the robustness of the defect state [i.e., both the position of the eigenfrequency $\nu^D = \beta_0$ and the shape of the mode; see Eq. (2)] against structural disorder, we introduced random variations of the coupling strengths t_1 and t_2, while preserving the dimer structure of the lattice; see Fig. 1(c). To this end, we have replaced each of the values of t_n in Eq. (1) with a random statistically independent coupling given by $t_{1/2} \to \tilde{t}_{1/2} = t_{1/2} + \frac{W}{2}\xi_n\tilde{t}$, where W is the disorder strength, and ξ_n is a random number drawn from a uniform distribution in the interval $[-1,1]$. Finally, $\tilde{t} = \frac{t_1 - t_2}{2}$. We note that a detailed experimental study of the robustness of the topologically protected defect mode has been performed in [21]. It turns out (see next section) that the resilience of the topologically protected mode carries over also in the case when the system is coupled to two leads. In this case, the defect mode becomes a topologically protected resonant mode, giving rise to a robust (against structural disorder) resonant transmittance; see Fig. 1(d).

Let us now assume that the central resonator is made by a nonlinear material (say with a Kerr-like or thermal nonlinearity), thus making it more susceptible (with respect to the other resonators) to incident light radiation. In this case its permittivity, and consequently its resonant frequency β_0, will be modified as $\beta_{11} = \beta_0 \to \beta_0 + \delta$ whenever the power or fluence of the incident radiation is above some critical value. We find that the small detuning δ will formally induce a

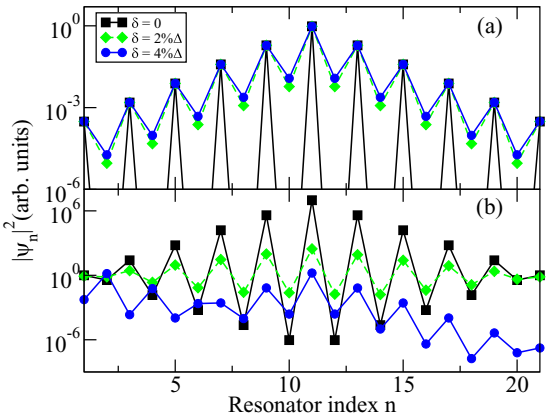

FIG. 2. (a) Defect mode profiles of the $\mathcal{CT}$-symmetric CROW of Eq. (1) for various detuning strengths δ. As δ increases, the staggered form of the field is destroyed. (b) Scattering field distribution at resonant frequency for the same systems described in (a). Note the nonmonotonic field intensity vs δ at the position of the lossy resonators. Eventually the destruction of the resonant localized defect mode occurs.

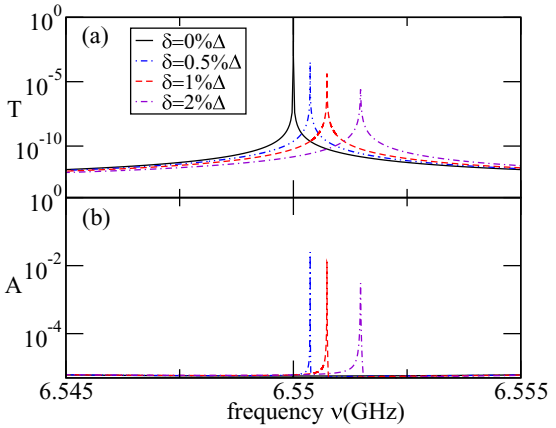

FIG. 3. (a) Transmittance (T), and (b) absorbance (A) vs frequency for various detuning strengths δ. The system is shown in Fig. 1(a).

violation of $\mathcal{C}$ symmetry for $H(0)$ as well as a violation of $\mathcal{CT}$ symmetry for $H(\gamma)$. Furthermore, at some critical value of δ the staggered form Eq. (2) of the defect mode ψ^D is destroyed, acquiring a nonzero field amplitude at the lossy resonators at $n = 10$ and $n = 12$; see Fig. 2(a). At the same time the associated eigenfrequency ν^D acquires an imaginary part—a signature of a low Q factor due to the local losses at resonators $n = 10$ and $n = 12$. Using second-order perturbation theory with respect to $P_{\{n=11\}}$ we estimate that for $\delta < 4t_1/N$ ($4t_1/N$ is the spacing between nearby levels for $\delta = 0$) the imaginary part of ν^D of the perturbed system $H(\gamma) + \delta P_{\{n=11\}}$ scales as $\mathrm{Im}\{\nu^D\} \propto \delta^2$.

III. HYPERSENSITIVE TRANSPORT

Next, we couple the system of Eq. (1) with two antennas, at the first and last resonators. The antennas are modeled as one-dimensional semi-infinite periodic tight-binding lattices with coupling constants $t_L = (t_1 + t_2)/2$ and on-site eigenfrequencies $\beta_L = \beta_0$. These antennas support propagating waves with an eigenfrequency $\nu = \nu_L - 2t_L \cos k$ where k is the associated wave vector. The coupling between the antennas and the first and last resonator is assumed to be t_L.

Within the scattering framework, the defect mode becomes a resonant localized mode with small but finite linewidth. Its shape and transport properties are studied using the transfer matrix M_n:

$$\begin{pmatrix} \psi_{n+1} \\ \psi_n \end{pmatrix} = M_n \begin{pmatrix} \psi_n \\ \psi_{n-1} \end{pmatrix}, \; M_n \equiv \begin{pmatrix} \frac{\nu-\beta_n}{t_{n+1}} & -\frac{t_n}{t_{n+1}} \\ 1 & 0 \end{pmatrix}. \quad (3)$$

Equation (3), together with appropriate boundary conditions, allows us to obtain the resonant mode profile at any resonator within the CROW. Without loss of generality we shall use the scattering boundary conditions $\psi_n = te^{ink}$ for $n \geqslant N$ and $\psi_n = e^{ink} + re^{-ink}$ for $n \leqslant 1$ describing a left incident propagating wave with unit amplitude and reflection coefficient r. The associated transmittance $T = |t|^2$ and reflectance $R = |r|^2$ are evaluated via iteration of Eq. (3).

The scattering field intensities of the resonant defect mode for different values of the detuning δ are shown in Fig. 2(b). When $\delta = 0$, the scattering field profile resembles the staggered form Eq. (2) of the associated localized defect mode. Importantly, the position of the lossy resonators at $n = 10$, 12 coincides with the position of the (quasi-)nodal points of the resonant defect mode. Thus, the interaction of the field with these cavities is negligible and the structure demonstrates the phenomenon of "*symmetry-enforced transmittivity*"; i.e., we have a high resonant transmission peak at $\nu = \nu_0$; see Fig. 3(a). The spectral position of the resonant transmission peak is robust against positional disorder, as is demonstrated in Fig. 1(d).

When a small detuning δ is introduced, the $\mathcal{CT}$ symmetry is violated and the field amplitudes at the lossy resonators at sites 10 and 12 are different than zero; see Fig. 2(b). At the same time the resonant transmission peak decreases; see Fig. 3(a). Interestingly enough, also the absorbance shows the same decreasing trend; see Fig. 3(b) and discussion below. For even larger values of δ, the resonant localized mode is suppressed and for $\delta = \delta_{\mathrm{crit}}$ it is eventually destroyed; see Fig. 2(b). One can estimate this critical detuning by realizing that the destruction of the resonant mode is associated with the competition between two physical mechanisms: the deterioration of the resonant Q factor because of the radiative losses from the boundary which lead to broadening of the linewidth by $\Gamma_{\mathrm{rad}} \propto \exp(-N/\xi)$, and the bulk (Ohmic) losses which are triggered by the interaction of the field with the lossy resonators at sites 10 and 12. The latter contributes to a linewidth $\mathrm{Im}\{\nu^D\} \propto \delta^2$(see previous discussion). Equating these two expressions we obtain $\delta_{\mathrm{crit}} \propto \exp(-N/2\xi)$. In other words, even an exponentially small detuning results in the destruction of the resonant defect mode and a dramatic suppression of the associated resonant transmittance; see Fig. 4(a). The underlying physical mechanism associated with this abrupt change in the transport characteristics of the photonic structure relies on an underdamping-to-overdamping transition. In the former regime, the (small) radiative losses are the dominant

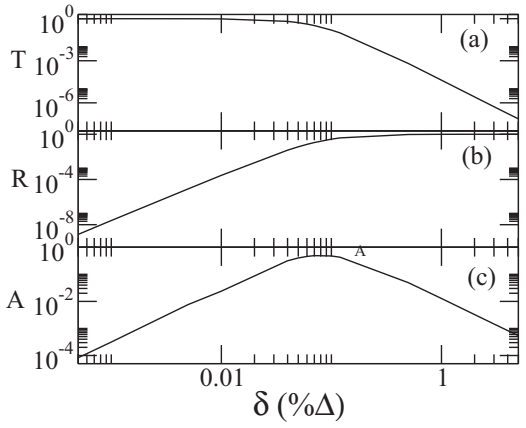

FIG. 4. (a) The resonant transmittance T, (b) reflectance $\boldsymbol{R}$, and (c) absorbance $\boldsymbol{A}$ vs the detuning strength $\boldsymbol{\delta}$.

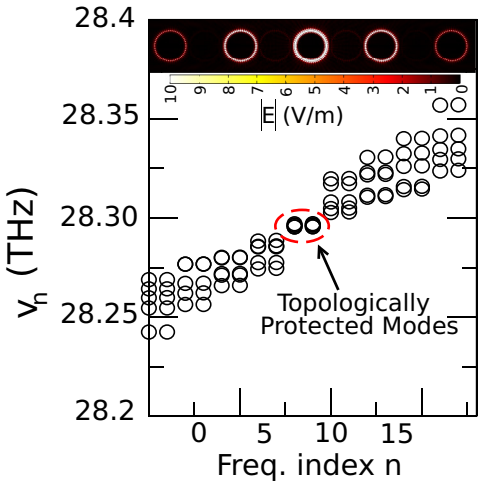

FIG. 5. Frequency spectrum for various realizations of random distances $\boldsymbol{d_1}$, $\boldsymbol{d_2}$ of a $\mathcal{CT}$-symmetric CROW consisting of nine rings. The two (quasidegenerate) defect modes in the middle of the gap remain unaffected by the disorder and preserve the staggered form of Eq. (2) (see inset for a density plot— even rings are not visible).

mechanism that spoils the Q factor of the structure, while in the latter case the Q factor is dominated by the (strong) Ohmic losses. In this case, there is a strong impendence mismatch between the incoming wave and the resonant defect mode which, in turn, leads to the high reflection and consequently suppressed transmittance observed in our simulations.

In Figs. 4(b) and 4(c), we report the reflectance and absorbance at the associated resonant frequency, vs the detuning δ. We find that, for $\delta \approx \delta_{\rm crit}$, the incoming photons do not couple at all with the resonant mode (strong impedance mismatch), but rather are reflected immediately. A quantitative understanding of this behavior requires the analysis of the absorbance $A(\nu)$ of the resonance mode. Using Eq. (3) we obtain

$$\sum_{n=1}^{N} \gamma_n \left|\psi_n^\delta\right|^2 + t_L \mathrm{Im}\left\{\left(\psi_1^\delta\right)^* \psi_0^\delta + \left(\psi_N^\delta\right)^* \psi_{N+1}^\delta\right\} = 0, \qquad (4)$$

where ψ_n^δ is the nth component of the scattering field associated with a detuning δ and we have used the fact that the frequency $\nu(k)$ of the incident wave is real. Substituting in Eq. (4) the expressions of the field $\psi_n = te^{ink}$ for $n \geqslant N$ and $\psi_n = e^{ink} + re^{-ink}$ for $n \leqslant 1$, and taking into consideration that $\gamma_n = \gamma$ for $n = 10,\ 12$, and zero otherwise, we obtain

$$A \equiv 1 - T - R = 2\gamma \frac{\left|\psi_{10}^\delta\right|^2 + \left|\psi_{12}^\delta\right|^2}{v_g}, \qquad (5)$$

where $v_g = \partial\nu(k)/\partial k$ is the group velocity. From Eq. (5) one concludes that the absorbance depends on the (Ohmic) dissipation γ, the value(s) of the scattering field intensities at the position of the dissipative resonators, and is inversely proportional to the group velocity $v_g(k)$. In our case, γ is constant. At the same time, $v_g(k)$ at the resonant mode can also be considered constant, to a good approximation (a small shift of the resonant position $\sim \delta$ is irrelevant for our discussion).

On the other hand, the change of the scattering field intensities $|\psi_{10}^\delta|^2$, $|\psi_{12}^\delta|^2$ can vary by orders of magnitude as δ increases; see Fig. 2(b). Specifically, for $\delta = 0$ we have $|\psi_{10}^\delta|^2, |\psi_{12}^\delta|^2 \approx 0$ and thus $A = 0$. For small detuning strengths $\delta < \delta_{\rm crit}$, the scattering field intensities $|\psi_{10}^\delta|^2$, $|\psi_{12}^\delta|^2$ increase [see $\delta = 2\%$ in Fig. 2(b)] and as a result the absorbance A also increases [see Fig. 4(c)]. However, when $\delta > \delta_{\rm crit}$ the field intensities at $n = 10,\ 12$ begin to decrease [see $\delta = 4\%$ in Fig. 2(b)] due to the destruction of the resonant defect mode (see previous discussion). As a result, we expect from Eq. (5) that the absorbance A will decrease to zero [see Fig. 4(c)]. Consequently, the reflectance $R \equiv 1 - T - A$ reaches values close to unity.

IV. ON-CHIP OPTICAL CROWs WITH SELF-INDUCED VIOLATION OF $\mathcal{CT}$ SYMMETRY

We have also considered a $\mathcal{CT}$-symmetric CROW array consisting of $N = 9$ coupled optical rings, placed at alternate distances $d_1 = 35.54\ \mu$m, $d_2 = 36.4\ \mu$m. The defect ring resonator is located at the center of the chain at a distance d_2 from the adjacent resonators; see Fig. 5. Each ring resonator supports a clockwise (CW) and a counterclockwise (CCW) degenerate mode. The array can be theoretically investigated using a coupled mode theory. The associated Hamiltonian is given by Eq. (1) with

$$\beta_n \to \hat{\beta}_n = \begin{pmatrix} \beta_n^{\rm CW} & 0 \\ 0 & \beta_n^{\rm CCW} \end{pmatrix};\ t_n \to \hat{t}_n = t_n \begin{pmatrix} 0 & 1 \\ 1 & 0 \end{pmatrix}, \qquad (6)$$

where $\beta_n^{\rm CW/CCW} = 28.3$ THz are the degenerate eigenfrequencies of the CW and CCW modes of the nth ring. Hamiltonian (1) with Eq. (6) satisfy the $\mathcal{CT}$ symmetry and has two quasidegenerate topologically protected defect modes.

In our simulations below we have assumed that the rings are made of Si ($\epsilon_{Si} = 10.89$) while the cladding is made of SiO_2 ($\epsilon_{SiO_2} = 4$). The defect resonator consists of a material with a temperature-dependent permittivity. In our numerical example, we have assumed that $\epsilon_d(\theta) = \epsilon_0[1 + 3/(e^{-[\theta-\theta_0]/5\rm K} + 1)]$, where $\theta_0 = 342$ K and $\epsilon_0 = \epsilon_{\rm Si}$. We note that this temperature-dependent permittivity has been extracted from experimental measurements and it is associated with a VO_2 material in the midinfrared (MIR) regime [42]. Finally, the lossy rings at the left and right of the central resonator have complex permittivity

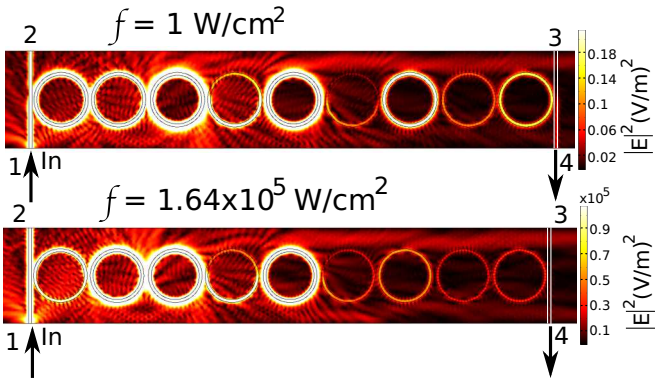

FIG. 6. The density plot of the scattering electric field intensity profiles displayed for the case when the CROW photonic structure with $\mathcal{CT}$ symmetry is irradiated with a low (high) fluence incident wave.

$\epsilon_{\text{lossy}} = 10.89 + 0.162\,85i$. Using COMSOL'S eigenmode routine we evaluate the CROW's frequency spectrum associated with the fundamental mode of the individual resonators. The degenerate defect modes at the middle of the band gap (see Fig. 5) have the typical staggered form imposed by the $\mathcal{CT}$ symmetry (see inset of Fig. 5) and they are spectrally protected against positional disorder (i.e., random d_1, d_2) as long as the bipartite nature of the CROW is preserved.

Next, we evanescently couple the first and last ring with a Si bus waveguide and study the transmittance $T \equiv |S_{31}|^2 + |S_{41}|^2$, and reflectance $R = |S_{11}|^2 + |S_{21}|^2$ of an incident wave from port 1 (associated with the left bus waveguide). The scattering parameters S_{31}, S_{41} describe transmission amplitudes from port 1 to ports 3 and 4 of the right waveguide, while S_{11}, S_{21} describe transmission amplitudes from port 1 to port 2 and back to port 1 of the left waveguide (see top and bottonsetsm of Fig. 6). Since there are intrinsic radiative losses we evaluate the Ohmic absorption (due to the metallic rings) directly via the expression $A = \frac{\nu}{2} \int d^3\vec{r} |E(\vec{r})|^2 \epsilon''(\vec{r})$ [43]. The scattering parameters and the steady-state scattering field $E(\vec{r})$ associated with an incident monochromatic wave at frequency ν are calculated using the Maxwell's equations coupled with the heat transport equations that dictate the steady-state temperature $\theta(\vec{r})$ within the CROW array:

$$\nabla^2 \vec{E} + \mu_0 \epsilon(\vec{r},\theta) \nu^2 \vec{E} = 0, \; \nabla \cdot [\kappa(\vec{r}) \nabla \theta(\vec{r})] = Q, \quad (7)$$

where $\epsilon(\vec{r},\theta) = \epsilon'(\vec{r},\theta) + i\epsilon''(\vec{r})$ is the permittivity of the CROW array at position z and steady-state temperature θ and $\epsilon''(\vec{r}) = \sigma(\vec{r})/\omega$. The portion of the incident radiation which is absorbed by the defect resonator leads to a gradual heating of this resonator. This temperature increase, in turn, leads to a variation of the permittivity as we discussed above. Therefore, one needs to solve simultaneously the Maxwell's and heat-transfer equations in a self-consistent manner in order to achieve steady-state transmittance, reflectance, and absorbance of the CROW array. Furthermore, we have assumed a fixed ambient temperature (293 K) at the boundaries surrounding the SiO_2 cladding. The parameter $Q = 0.5 \times \text{Re}(\vec{J} \cdot \vec{E})$, where $\vec{J} = \sigma \vec{E}$, describes the electromagnetic energy deposited at the lossy metal-coated rings adjacent to the defect ring resonator

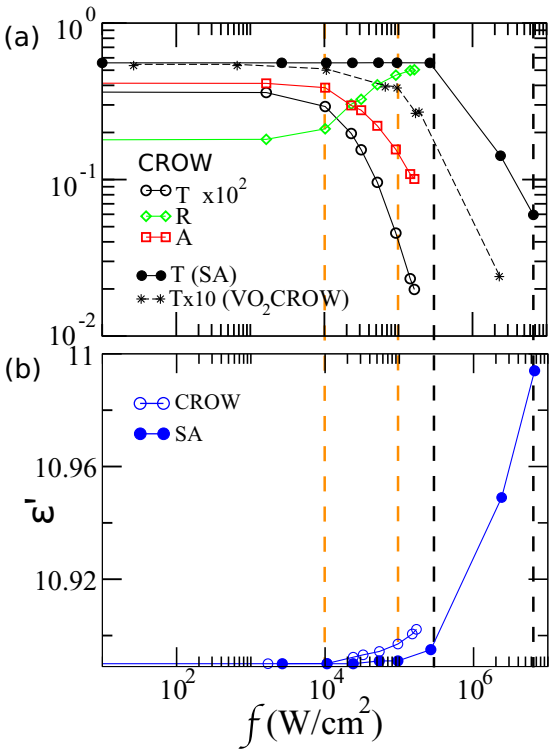

FIG. 7. (a) The transmittance T, reflectance R, and absorbance A, evaluated for the proposed CROW photonic structure with $\mathcal{CT}$ symmetry (empty symbols), obtained using COMSOL MULTIPHYSICS software. The transmittance T is compared with that of a stand-alone (SA) ring resonator made of the same highly thermal nonlinear material (VO_2) (filled circles) and with an array of VO_2-based nonlinear resonators (dashed line with stars). In our case, the limiting threshold is achieved at incident fluences which are at least one order smaller than that required for the SA ring resonator (compare leftmost black and orange vertical dashed lines). Similarly, the limiting threshold for the VO_2 CROW is achieved for fluencies which are at least one order higher than the ones of our proposed CROW array (not marked in the figure). The two vertical orange (black) lines indicate the borders for which transmittance at the CROW (SA ring resonator) drops by an order, for an order (almost two orders) increase in incident fluence. (b) Thermally induced change in real permittivity of the defect ring resonator in the case of the CROW photonic structure (empty symbols) and SA ring-resonator structure (solid symbols).

which leads to an increase in temperature θ. Finally, $\kappa(\vec{r})$ denotes the thermal conductivity of the rings making up the CROW array structure.

The upper (lower) panel of Fig. 6 shows the density plot of the scattering electric field intensity for incident signals with small (large) fluence. In the former case, the profile of the resonant defect mode respects the staggered form imposed by $\mathcal{CT}$ symmetry. In contrast, in the latter case (lower panel of Fig. 6), the staggered profile is completely destroyed, thus leaving the defect mode exposed to the metallic resonators. In this case, the resonant transmission is completely suppressed. In Figs. 7(a) and 7(b), we report T, R, A, and $\epsilon_d(\theta)$ vs incident fluences for the CROW array (empty symbols). We observe that when the fluence of the incident light increases by an order of magnitude [i.e., from 10^4 to 10^5 W/cm^2—see vertical orange

lines in Fig. 7(a)] the resonant transmission is also suppressed by an order. In Fig. 7(b), we also report the tiny relative permittivity variations ($\sim$0.1%) which are associated with the increase of fluence of the incident light [see dashed vertical orange lines in Fig. 7(b)], due to the self-induced heating at the defect resonator caused by the incident radiation. Similarly, the Ohmic absorption A decays as the fluence increases, thus protecting the CROW from self-damaging due to overheating. At the same time the reflectance R increases as high as $\sim$0.55. Note that R does not reach unity because there is a strong residual radiative absorption in the bus waveguide ($A \sim 0.4$).

For comparison purposes, we also show in the same figure the transmittance T and the permittivity variation $\epsilon_d(\theta)$ vs incident fluences for the case of a stand-alone (SA) ring resonator (filled circles) made by the same material (VO_2) as the defect resonator of the CROW arrangement. The resonator is now directly coupled to the bus waveguides. A similar SA resonator setup has been already investigated in Ref. [44] where it was shown experimentally that it can act as an on-chip limiter. The limiting action mechanism in this case relies on a resonant redshift—thus leaving the sensitive photonic elements exposed to damage in case of high-power broadband signal attacks. For extremely high fluencies the on-resonant transmittance is also suppressed due to an excessive heating which can lead to damage of the resonator [see Fig. 7(a)]. Conversely our design relies on complete suppression of the resonant mode at moderate fluences, thus protecting sensitive elements from any broadband (up to the size of the band gap) incident signal. In comparison, a complete resonant suppression in the case of the SA resonator requires a relative permittivity variation which is more than 1% (see the transmittance drop between the two black dashed lines in Fig. 7), which has to be compared with the 0.1% permittivity variation needed in the case of the CROW structure. Finally, we mark that our design demonstrates a limiting threshold (i.e., fluence value for which the transmittance drops to small values), which is smaller by an order of magnitude as compared to the SA ring-resonator structure; see Fig. 7(a). For completeness, we also compare the limiting performance of our photonic limiter with a CROW array consisting of the same number of VO_2-based resonators [dashed-star line in Fig. 7(a)]. The behavior of the latter is qualitatively similar to the one associated with the SA resonator. We find again that our CROW limiter has a lower (at least by an order) damage threshold.

V. CONCLUSION

We have investigated topologically protected defect modes and the transport properties of the associated resonant modes emerging in the frame of non-Hermitian bipartite CROW arrays. We show that an underlying $\mathcal{CT}$ symmetry enforces high resonant transmission and protects the resonant mode from positional disorder or local Ohmic losses that can potentially degrade the transport. When, however, a (self-)induced violation of $\mathcal{CT}$ symmetry occurs due to tiny variations of the permittivity of the defect, the resonant mode is destroyed and the transmission is completely suppressed. The fragile nature of resonant transport has been demonstrated for on-chip photonic and microwave CROW setups. Furthermore, it can be utilized in a variety of other frameworks including rf and acoustics for the realization of a different class of power limiters, switches, sensors, and modulators as well as for matter waves circuitry.

Finally, we want to stress that the underlying physical mechanism invoked in this study is completely different from the one utilized in Ref. [20] for suppressing high-power signals. In the latter case, for low incident field intensities or fluences, the system was chiral symmetric (not $\mathcal{CT}$ symmetric), and for high incident intensities or fluences one needed to utilize the presence of a strong nonlinear lossy mechanism in order to spoil the resonant Q factor. Such strong nonlinear mechanisms are typically hard to realize in the microwave domain and require high incident field intensities or fluences in order to be activated. Here, instead, the structure is initially respecting a $\mathcal{CT}$ symmetry which guarantees the existence of high transmittivity for low incident field intensities or fluences via the phenomenon of symmetry-enforced transmittivity. In the opposite limit of high incident field intensities or fluences, the abrupt drop of transmittance is triggered by the self-induced violation of $\mathcal{CT}$ symmetry which is achieved via (weak) nonlinear effects that change the value of the permittivity (for very small incident field powers) of the defect resonator by one to two percentage points—or even less.

ACKNOWLEDGMENTS

We acknowledge partial support from Office of Naval Research (ONR) via Grant No. N00014-16-1-2803, from Air Force Office of Scientific Research (AFOSR) MURI Grant No. FA9550-14-1-0037, and from National Science Foundation (NSF) via Grant No. EFMA-1641109.

[1] R. P. Feynman, R. B. Leighton, and M. Sands, *The Feynman Lectures on Physics* (Basic Books, New York, 2011), Vol. III.

[2] B. A. van Tiggelen, *Serguei Skipetrov, Wave Scattering in Complex Media: From Theory to Applications* (Springer Science & Business Media, New York, 2003).

[3] Y. V. Nazarov and Y. M. Blanter, *Quantum Transport: Introduction to Nanoscience* (Cambridge University Press, Cambridge, 2009).

[4] B. E. A. Saleh and M. C. Teich, *Fundamentals of Photonics* (Wiley, New York, 1991).

[5] R. Thomas, H. Li, F. M. Ellis, and T. Kottos, Phys. Rev. A **94**, 043829 (2016).

[6] H. Li, R. Thomas, F. Ellis, and T. Kottos, New J. Phys. **18**, 1367 (2016).

[7] J. J. M. Verbaarschot and I. Zahed, Phys. Rev. Lett. **70**, 3852 (1993).

[8] J. J. M. Verbaarschot and T. Wettig, Annu. Rev. Nucl. Part. Sci. **50**, 343 (2000).

[9] A. Altland and M. R. Zirnbauer, Phys. Rev. B **55**, 1142 (1997).

[10] L. Lu, J. D. Joannopoulos, and M. Soljacic, Nat. Photonics **8**, 821 (2014).

[11] S. Raghu and F. D. M. Haldane, Phys. Rev. A **78**, 033834 (2008).
[12] Z. Wang, Y. Chong, J. D. Joannopoulos, and M. Soljacic, Nature (London, U. K.) **461**, 772 (2009).
[13] M. Hafezi, E. A. Demler, M. D. Lukin, and J. M. Taylor, Nat. Phys. **7**, 907 (2011).
[14] K. Fang, Z. Yu, and S. Fan, Nat. Photonics **6**, 782 (2012).
[15] T. Kitagawa, M. A. Broome, A. Fedrizzi, M. S. Rudner, E. Berg, I. Kassal, A. Aspuru-Guzik, E. Demler, and A. G. White, Nat. Commun. **3**, 882 (2012).
[16] A. B. Khanikaev, S. H. Mousavi, W.-K. Tse, M. Kargarin, A. H. MacDonald, and G. Shvets, Nat. Mater. **12**, 233 (2013).
[17] M. Hafezi, S. Mittal, J. Fan, A. Migdall, and J. M. Taylor, Nat. Photonics **7**, 1001 (2013).
[18] M. C. Rechtsman, J. M. Zeuner, Y. Plotnik, Y. Lumer, D. Podolsky, F. Dreisow, S. Nolte, M. Segev, and A. Szameit, Nature (London) **496**, 196 (2013).
[19] J. Arkinstall, M. H. Teimourpour, L. Feng, R. El-Ganainy, and H. Schomerus, Phys. Rev. B **95**, 165109 (2017).
[20] U. Kuhl, F. Mortessagne, E. Makri, I. Vitebskiy, and T. Kottos, Phys. Rev. B **95**, 121409(R) (2017).
[21] C. Poli, M. Bellec, U. Kuhl, F. Mortessagne, and H. Schomerus, Nat. Commun. **6**, 6710 (2015).
[22] R. El-Ganainy and M. Levy, Opt. Lett. **40**, 5275 (2015).
[23] X.-L. Qi and S.-C. Zhang, Rev. Mod. Phys. **83**, 1057 (2011).
[24] D. Pikulin and Y. Nazarov, JETP Lett. **94**, 693 (2012).
[25] D. I. Pikulin and Y. V. Nazarov, Phys. Rev. B **87**, 235421 (2013).
[26] M. Parto, S. Wittek, H. Hodaei, G. Harari, M. A. Bandres, J. Ren, M. C. Rechtsman, M. Segev, D. N. Christodoulides, and M. Khajavikhan, Phys. Rev. Lett. **120**, 113901 (2018).
[27] S. Weimann, M. Kremer, Y. Plotnik, Y. Lumer, S. Nolte, K. G. Makris, M. Segev, M. C. Rechtsman, and A. Szameit, Nat. Mater. **16**, 433 (2017).
[28] Z. M. Hasan and C. L. Kane, Rev. Mod. Phys. **82**, 3045 (2010).
[29] H. Zhao, P. Miao, M. H. Teimourpour, S. Malzard, R. El-Ganainy, H. Schomerus, and L. Feng, Nat. Commun. **9**, 981 (2018).
[30] P. San-Jose, J. Cayao, E. Prada, and R. Aguado, Sci. Rep. **6**, 21427 (2016).
[31] S. Malzard, C. Poli, and H. Schomerus, Phys. Rev. Lett. **115**, 200402 (2015).
[32] H. Schomerus, Opt. Lett. **38**, 1912 (2013).
[33] Y. V. Fyodorov and Alexander Ossipov, Phys. Rev. Lett. **92**, 084103 (2004).
[34] H. Schomerus, M. Marciani, and C. W. J. Beenakker, Phys. Rev. Lett. **114**, 166803 (2015).
[35] E. Makri, H. Ramezani, T. Kottos, and I. Vitebskiy, Phys. Rev. A **89**, 031802(R) (2014).
[36] E. Makri, T. Kottos, and I. Vitebskiy, Phys. Rev. A **91**, 043838 (2015).
[37] D. Lelmini and A. L. Lacaita, Mater. Today **14**, 600 (2011).
[38] G. Stefanovich, A. Pregament, and D. Stefanovich, J. Phys.: Condens. Matter **12**, 8837 (2000).
[39] S. D. Ha, Y. Zhou, C. J. Fisher, S. Ramanathan, and J. P. Treadway, J. Appl. Phys. **113**, 184501 (2013).
[40] J. K. Asboth, L. Oroszlany, and A. Palyi, *A Short Course on Topological Insulators*, Lecture Notes in Physics 919 (Cambridge University Press, Cambridge, 2016).
[41] L. Ge, Phys. Rev. A **95**, 023812 (2017).
[42] M. A. Kats, R. Blanchard, P. Genevet, J. Lin, D. Sharma, Z. Yang, M. M. Qazilbash, D. Basov, S. Ramanathan, and F. Capasso, Opt. Lett. **38**, 368 (2013).
[43] R. Thomas, L. Fabris, and D. M. O'Carroll, Plasmonics **9**, 1283 (2014).
[44] S. Yan, J. Dong, A. Zheng, and X. Zhang, Sci. Rep. **4**, 6676 (2014).